Correlation between Chain Packing and Photoluminescence for PPV/PPE in Macroscopically Oriented State: Side Chain Effects†

Benjamin Carbonnier,‡,§ Daniel Ayuk Mbi Egbe,*,‖ Eckhard Birckner,⊥ Ulrich-Walter Grummt,⊥ and Tadeusz Pakula‡

Max-Planck-Institut für Polymerforschung, Ackermannweg 10, D-55021 Mainz, Germany, Institut für Organische Chemie und Makromolekulare Chemie, Humboldtstr. 10, D-07743 Jena, Germany, and Institut für Physikalische Chemie der Friedrich-Schiller Universität Jena, Lessingstrasse 10, D-07743 Jena, Germany

Received June 21, 2005; Revised Manuscript Received July 13, 2005

ABSTRACT: Self-organization features of poly(*p*-phenylene-vinylene)/poly(*p*-phenylene-ethynylene)s (PPV/PPE)s polymers of constitutional structure (−Ph−C≡C−Ph−C≡C−Ph−CH=CH−Ph−CH=CH−)$_n$ and bearing two alkoxy side chains on either every one (**1**) or every second (**2**) phenylene moieties are presented. Formation of self-assembled structures on various size scales has been examined using a combination of experimental methods. Initial investigations performed for macroscopically isotropic samples by means of DSC, POM, and 2D SALS have revealed a strong dependence of the thermal behavior and related morphologies on the side chain densities. The existence of organizational features in macroscopically oriented bulk samples (extruded filaments) was also demonstrated using 2D WAXS. Self-organization of (PPV/PPE)s into biphasic structures made of spatially segregated main chain layers with the side chains filling the space between layers was postulated. The local arrangement of the macromolecular subunits was strongly dependent on the macromolecular architecture and temperature. Two types of organization of the polymer chains assuming translationally correlated (**2**) and uncorrelated (**1**) positions could be distinguished. Fluorescence investigations using a frontal geometry setup were performed on the extruded filaments. Side-chain-dependent correlation between the structure and the photophysical behavior of PPV/PPE could be established for the uniaxial orientation showing the bathochromic shift of the emission peak with the decrease of the interchain distances within layers.

Introduction

Polymeric materials of well-defined macromolecular architecture made of structural subunits that are incompatible with each other have been considered as a very promising pathway for the formation of interesting materials with self-organization abilities on the molecular level. This kind of imposed chemical and geometrical anisotropy into unique covalently bonded macromolecular system allows a design of new materials with increased supramolecular ordering. A number of macromolecular systems have now been reported, including side chain,[1] main chain,[2] as well as combined side and main chain liquid crystalline polymers,[3] with different self-organizational behaviors[4] and advanced properties.[5]

Structural details of main chain liquid crystalline polymers may control the microphase separation, aggregation, and order−disorder phase transitions that are essential phenomena governing the arrangement of these rigid macromolecules into self-assembled layers.[6−9] To obtain rigid macromolecules with targeted properties, molecular architecture has been engineered by choosing the appropriate combination of main chain rigid repeating units and lateral flexible substituents, resulting in a wide range of "hairy-rod" macromolecules having the advantage of a facile color tunability, good film-forming properties, adequate mechanical properties, and potential applications in nanoscale photonic[10] and optoelectronic[11] devices such as light-emitting diodes,[12] light-emitting electrochemical cells,[13] field effect transistors,[14] lasers,[15] and organic solar cells.[16]

Poly(*p*-phenylene-vinylene)s (PPV)s[17−19] and their dehydrogenated congeners poly(*p*-phenylene-ethynylene)s (PPE)s are among the most promising π-conjugated polymeric materials for optoelectronic uses. Alkyl- and/or alkoxy-substituted hybrid *p*-phenylene-vinylene/*p*-phenylene-ethynylene polymers (PPV/PPE)s with a perfectly controlled ratio of the −C≡C− and −CH=CH− moieties have been synthesized with the aim of combining the interesting intrinsic properties of both classes of compounds into a single polymeric backbone,[20−23] and great attention has been devoted to the effects of the molecular features on their bulk structure and photophysical properties.[24]

Herein, we focus on thermal and structural analyses of (PPV/PPE)s **1** and **2** of well-defined backbone repeating unit (RU) (−Ph−C≡C−Ph−C≡C−Ph−CH=CH−Ph−CH=CH−)$_n$ and having eight (**1**) or four (**2**) alkoxy grafted side groups per RU (Scheme 1). (PPV/PPE)s **1** and **2** were obtained from the Horner−Wadsworth−Emmons[25] olefination reaction as previously described.[23c] Some molecular characteristics of polymers **1** and **2** are given in Table 1. Comparison of bulk properties of ten polymeric samples as investigated by means of differential scanning calorimetry (DSC), polarized optical microscopy (POM), two-dimensional small-angle light

† This work is dedicated to the late Prof. Dr. Tadeusz Pakula for his outstanding contributions in the field of polymer physics.

* Correspondence should be addressed to: phone (+49)-(0)-3641-948247; fax (+49)-(0)-3641-948202; e-mail c5ayda@uni-jena.de. E-mail addresses of the coauthors: carbonnier@glvt-cnrs.fr (B.C.), ceb@uni-jena.de (E.B.), cug@uni-jena.de (U.-W.G.).

‡ Max-Planck-Institut für Polymerforschung.

§ Present address: Laboratoire de Recherche sur les Polymères, CNRS-Université Paris XII, 2 rue Henri Dunant, Thiais 94320, France.

‖ Institut für Organische Chemie und Makromolekulare Chemie.

⊥ Institut für Physikalische Chemie der Friedrich-Schiller Universität Jena.

10.1021/ma0513160 CCC: $30.25
Published on Web 08/13/2005

Scheme 1

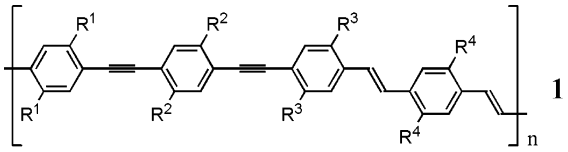

1

1a : $R^1 = R^3 =$ octyloxy, $R^2 = R^4 =$ (2-ethyl)hexyloxy
1b : $R^1 = R^3 = R^2 = R^4 =$ octyloxy
1c : $R^1 = R^3 = R^4 =$ octyloxy, $R^2 =$ octadecyloxy
1d : $R^1 = R^3 =$ octyloxy, $R^2 = R^4 =$ octadecyloxy

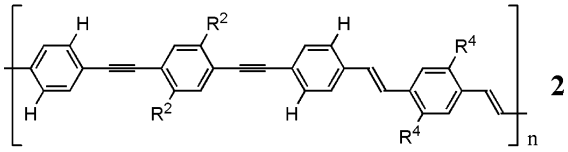

2

2a : $R^2 = R^4 =$ (2-ethyl)hexyloxy
2b : $R^2 =$ dodecyloxy, $R^4 =$ octadecyloxy
2c : $R^2 =$ octyloxy, $R^4 =$ octadecyloxy
2d : $R^2 =$ octadecyloxy, $R^4 =$ octyloxy
2e : $R^2 = R^4 =$ dodecyloxy
2f : $R^2 = R^4 =$ octadecyloxy

Table 1. Molecular Characteristics for the (PPV/PPE)s 1 and 2

PPV/PPE	Mw[a]	Mn[a]	Mw/Mn[a]	DP[a]
1a	77 200	15 400	5.0	11
1b	37 100	16 300	2.2	12
1c	82 500	29 400	2.8	17
1d	62 400	27 500	2.2	14
2a	161 700	35 200	4.5	38
2b	166 600	39 200	4.2	30
2c	156 900	50 000	3.1	42
2d	351 600	58 000	6.0	48
2e	552 000	88 100	6.2	77
2f	166 000	37 200	4.4	25

[a] From GPC with a UV detector and using THF as eluent and polystyrene as standard.

scattering (2D SALS), and two-dimensional wide-angle X-ray scattering (2D WAXS) experiments is reported, in order to highlight the effects of structural variations on thermal behaviors, crystalline morphologies, and three-dimensional macromolecular arrangements of **1** and **2**. Atomic force microscopy (AFM) was employed to image thin film surface topology of **2e**, as a representative example. Fluorescence behavior of extruded bulk conjugated materials as investigated through frontal geometry setup is discussed in correspondence to the X-ray results.

Experimental Section

Instrumentation. DSC experiments were conducted with cooling and heating rates of 10 K·min^{-1} using a Mettler 30 calorimeter with a cell purged with nitrogen. Calibration for the temperature and enthalpy changes was performed using indium as a standard.

POM observations were performed using a Zeiss microscope (D-7082) equipped with a temperature-controlled stage (Linkam TMS91/THM600) and a color digital camera (Hitachi KPD50).

2D SALS experiments were conducted with a He−Ne laser (λ = 633 nm) beam and a CCD camera (Hamamatsu C-4880) recording the scattering 2D patterns under crossed ($h\nu$) polarization conditions. Temperature-dependent SALS measurements were performed using a sample stage (Linkam THMS 600) coupled with a programmable temperature control unit (Linkam 90).

WAXS 2D patterns were recorded using the X-ray beam with a pinhole collimation and a two-dimensional detector (Siemens Serial A102647) with 1024 × 1024 pixels. A double graphite monochromator for the CuKα radiation ($\lambda = 0.154$ nm) was used. The beam diameter was about 0.5 mm, and the sample to detector distance was 83.5 mm. Measurements were performed for cylindrical filaments with a thickness of about 0.7 mm. The filaments were obtained by means of microextrusion in a temperature range where polymers are plastically deformable. The patterns were recorded with vertical orientation of the filament axis and with the beam perpendicular to the filament. The recorded scattered intensity distributions were integrated over the azimuthal angle or along the equatorial (horizontal) and meridional (vertical) directions and are presented as functions of the scattering vector ($s = 2 \sin \theta/\lambda$, where 2θ is the scattering angle).[26]

AFM images were obtained by using a nanoscope IIIa multimode scanning probe microscope of Digital Instruments at room temperature. Measurements were carried out in tapping mode for samples spin-coated from toluene solution on graphite substrate with freshly cleaved surface.

Fluorescence measurements were performed with the help of a CD900 FS fluorescence spectrometer (Edinburgh Analytical Instruments) with a tungsten halogen lamp as excitation source. The polymer fibers were fixed onto a support and put into the spectrometer with the fiber axis parallel to the monochromator slits. The samples prepared exhibited a very large absorbance, and consequently, pre- and post-filter effects together with the measuring geometry chosen remarkably influenced the form of the spectra due to the cylindrical sample shape. To minimize these effects, the samples were measured with *frontal geometry,* and the emission was collected at 45° with respect to the direction of the excitation beam. The slit width of the excitation monochromator was adjusted in a way that a well-defined fraction of 5 mm of the particular fiber was completely illuminated. Plane sections (5 × 0.7 mm^2) of about 10-mm thickness obtained by microtome slicing (HM355 Microm) of the extruded bulk specimens along the filament axes were also investigated. These microtome-sliced specimens were adhered to a plane glass support and measured in the same way as the cylindrical filaments.

Results and Discussion

Thermal and Morphological Analyses. DSC and POM were used as complementary methods for the thermal and phase analyses of (PPV/PPE)s. The results revealed major differences between eightfold (**1**) and fourfold (**2**) alkoxy-substituted (PPV/PPE)s. The number, length, geometry, and location of substituents affect not only the transition temperatures but also the number and enthalpy of transitions observed. (PPV/PPE)s **1** undergo an endothermic transition upon heating at temperatures above 440 K (Figure 1). The transition temperatures decreased from **1b** to **1d** with the increase of the length of the side chains. On the basis of optical microscopic observations, these transitions were attributed to the melting of the materials from birefringent solids to isotropic liquids. Isotropization processes were detected better in the first heating

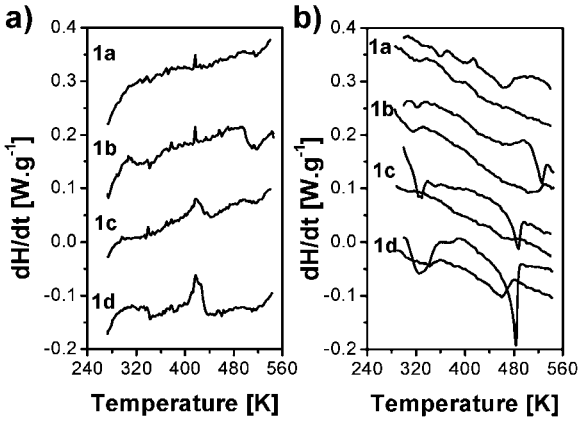

Figure 1. DSC thermograms recorded for the (PPV/PPE)s **1** during (a) cooling and (b) heating with the rate of 10 K/min. Both first (upper) and second (lower) heating runs are shown.

cycle, suggesting that the reorganization ability of **1** upon a rather fast cooling rate (10 K·min^{-1}) is limited. This is further confirmed by the weakly recorded crystallization processes. The effect of crystal growth conditions on developed morphology has also been examined. As examples, intermediate stage morphologies observed for **1b**, crystallized under non-isothermal and isothermal conditions, can be viewed in the upper left and upper right-hand sides of Figure 2, respectively. In both cases, speckle patterns were seen at the early stages of solidification processes, where birefringent domains of nearly spherical shape were seen randomly distributed over the whole field of view. The size of birefringent domains was observed to grow slighty upon further cooling or with crystallization time. This shows that structure formation from the polymer melt goes by nucleation and growth. However, the observed morphologies were weakly influenced by thermal treatment, and high nucleation rates were obtained in all cases. By employing cross-polarized 2D SALS experiments under similar conditions as for the microscopic observations, anisotropic patterns with azimuthal distribution of the scattered intensity characteristic for spherulitic superstructures were obtained.[27] An example of such a pattern can be viewed in the lower part of Figure 2 for **1b**. The average size of the spherulites was found to vary in the range between 5 and 12 μm for **1**. Endothermic transitions were observed in a lower temperature range (below ~450 K) for (PPV/PPE)s **2** (Figure 3). Upon cooling, **2** revealed exothermic processes occurring with considerable undercooling. Similarly to the thermal traces recorded for **1a**, 2-ethylhexyl-substituted polymer **2a** did not reveal any pronounced order−disorder transition. This suggests that space requiring branched substituents constitutes a limiting factor to the reorganization ability of (PPV/PPE)s polymeric materials. In contrast to the cases of polymers **1**, less densely substituted (PPV/PPE)s **2** underwent thermal decomposition before reaching isotropization temperatures. The interchain interactions are considerably increased in the cases of **2** because of the lower density of the diluting side chains. No textures typical for crystalline or liquid crystalline phases could be assigned to (PPV/PPE)s **2** from the POM observations. In most cases, melting and crystallization DSC peaks are broad and asymmetric. However, **2e** bearing four dodecyloxy substituents exhibits two well-defined first-order reversible transitions. The low- and high-temperature solid−solid-phase transitions are presumed to reflect the order−disorder

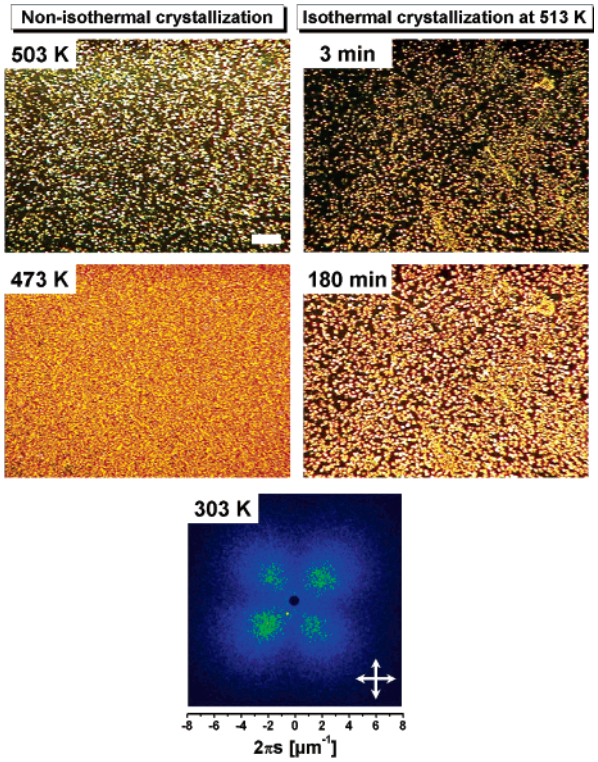

Figure 2. POM morphological observations for polymer **1b** thin film: (upper left) crystallized under non-isothermal conditions at temperatures of 503 and 473 K during cooling with a 10 K/min rate from isotropic melt and (upper right) crystallized under isothermal conditions at a temperature of 513 K for 3 and 180 min. The white bar in the upper left figure represents size of 100 μm. The lower part of the figure shows the $h\nu$ SALS 2D pattern as recorded for **1b** at room temperature after the non-isothermal crystallization process described above. The scale shown below represents the range of scattering vector values. The arrows in the $h\nu$ SALS 2D pattern indicate the polarization axes.

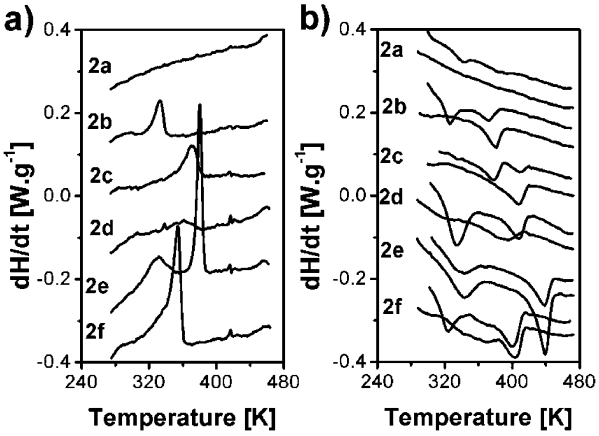

Figure 3. DSC thermograms recorded for the (PPV/PPE)s **2** during (a) cooling and (b) heating with the rate of 10 K/min. Both first (upper) and second (lower) heating runs are shown.

transitions of the side chains and main chains, respectively. Such thermal behavior suggests that both PPV/PPE backbones and dodecyloxy side chains are well-decoupled and may undergo thermal transition in a relatively independent way. These preliminary results on the phase behaviors and self-ordered morphologies of (PPV/PPE)s **1** and **2** as examined on a macroscopic level clearly show that order−disorder phenomena including isotropization, side chains and main chains

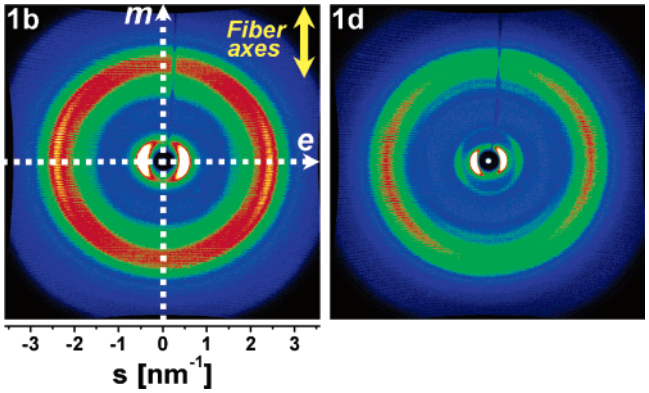

Figure 4. WAXS 2D patterns of oriented samples of **1b** and **1d** representative for (PPV/PPE)s of type **1**. Equatorial (e) and meridional (m) directions are indicated in the pattern by dashed horizontal and vertical lines, respectively. The scale shown below represents the range of scattering vector values and is valid for all the WAXS 2D patterns presented in this study.

melting, as well as crystallization are closely related to the RU molecular design.

Structural Analysis. (PPV/PPE)s **1** and **2** were processed at different temperatures using a microextrusion process to prepare macroscopically oriented filaments, and temperature-dependent structural parameters were extracted from their wide-angle X-ray patterns recorded using a 2D detector.[24i,28,29] In all cases, diffractions were seen in the low-angle equatorial region. These periodicities are presumed to result from nanoscale segregation between π-conjugated polymer backbones and aliphatic side chains that are immiscible with each other. They reflect the position correlations of self-ordered backbone domains along the transversal direction. The chain orientation is presumed to be along the drawing direction. Qualitative analysis of the X-ray fiber patterns revealed obvious structural differences between (PPV/PPE)s **1** and **2**.

(PPV/PPE)s **1** exhibited less ordered phases (Figure 4). Typically, a centrosymmetric broad halo was seen in the wide-angle region in addition to the equatorial reflections mentioned above. This indicates a liquidlike arrangement of the aliphatic segments within phase-separated domains. We presume that the scattered intensity maximum seen in the wide-angle equatorial area reflects the average interchain distance. (PPV/PPE)s **2** revealed more ordered structural phases with scattering effects depending on the molecular design of the RU. For **2a** that combines the lower number of side methylene groups and side chains with shortest linear parts (hexyloxy), the intense small-angle reflections along the equatorial direction indicate a good correlation between backbone-related structures (Figure 5). In contrast to that, **2f** having the longest side chains exhibits intensive reflections at wide angles along the meridional direction. This supports a good correlation of the side chains position along the direction parallel to the chain orientation. A major difference between (PPV/PPE)s **1** and **2** is that polymers **2**, when bearing linear groups, revealed periodicity along the backbone. The pattern presented in Figure 6, supported by the intensity distributions recorded along the equatorial and meridional directions shown below, demonstrate the highly ordered nature of **2e** at room temperature. The ordering along both directions parallel and perpendicular to the extrusion direction is clearly evidenced by the

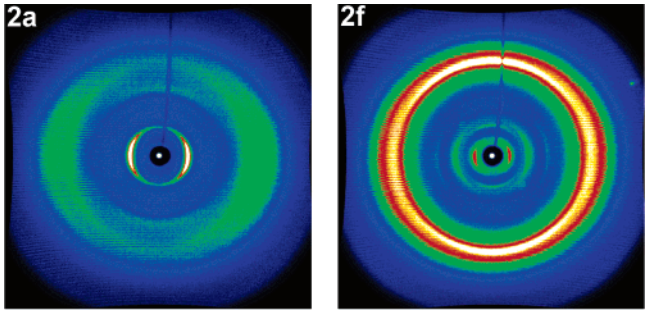

Figure 5. WAXS 2D patterns of oriented (PPV/PPE)s **2a** and **2f** samples. Scales and conditions the same as presented for Figure 4.

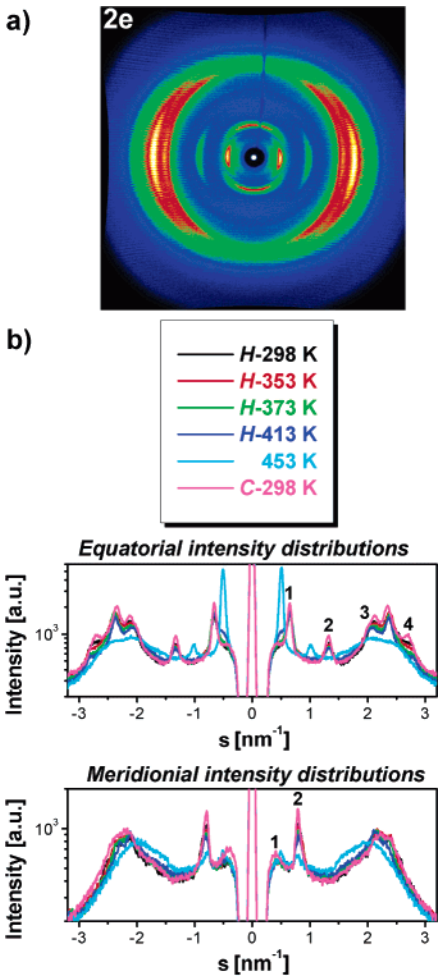

Figure 6. (a) WAXS 2D pattern of oriented (PPV/PPE) **2e** sample and (b) equatorial and meridional intensity distributions recorded for an oriented sample of **2e** at selected temperature during (H) heating and (C) cooling cycles.

following: (1) The equatorial reflections situated at s values satisfying the ratio 1:2:3:4 demonstrate the lateral ordering of the parallel-aligned chains into a layered structure, (2) the meridional reflections indicate dimensions which correlate well with the length of the chemical repeat unit within the chains and indicate that the positions of the chains are translationally correlated along the extrusion direction, and (3) the diffractions at wide angle are considered to reflect mainly the interchain correlations within the layers (along the equatorial direction) and the side chain crystallization. These periodicities as detected along 3D perpendicular to each other indicate that (PPV/PPE)s **2** with linear

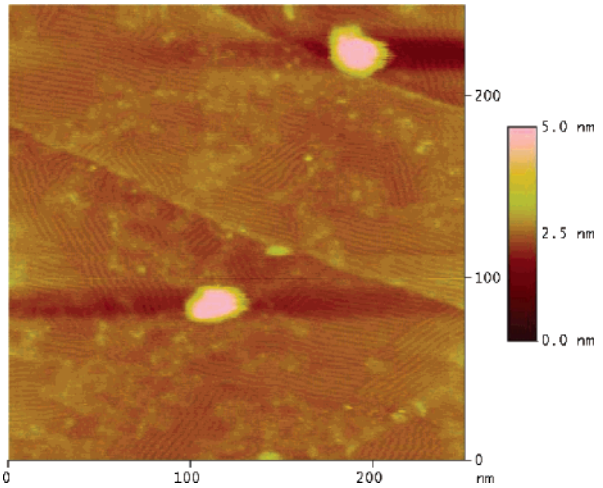

Figure 7. AFM image of **2e** thin polymer film showing layered polydomain surface topology.

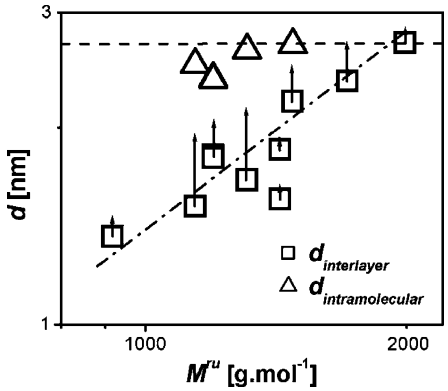

Figure 8. Dependence of (□) interlayer and (△) intramolecular periods extracted from the WAXS 2D patterns recorded for the macroscopically oriented (PPV/PPE)s **1** and **2** vs the molecular mass of the repeating units (M^{ru}). The lengths of the vertical arrows scale with the layer spacings increase observed at high temperature. The dashed−dotted line represents proportionality between $d_{interlayer}$ and M^{ru}. The horizontal dotted line reflects the predicted dimension for the (PPV/PPE)s repeating unit in fully extended conformation.

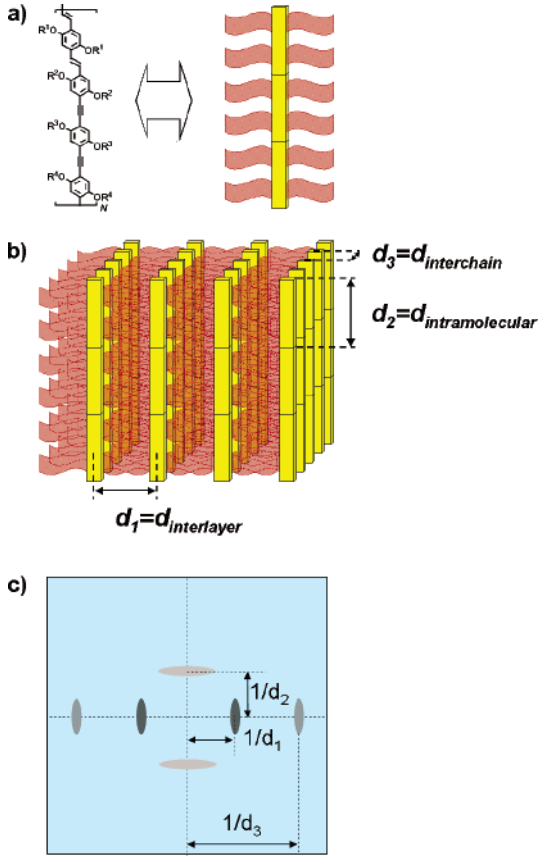

Figure 9. (a) Schematic representation of PPV/PPE with distinction of the only most important architectural units. (b) Schematic illustration of a 3D arrangement of bulk PPV/PPE in oriented state. The structure consists of main chain layers separated by the side chains. The experimentally detected characteristic distances corresponding to correlations between and within layers are also represented. (c) Schematic representation of a 2D fiber scattering pattern with contributions of effects related to structure considered in the part (b) of the figure. The reflections giving information about the dimensions $d_{interlayer}$ (d_1), $d_{intramolecular}$ (d_2), and $d_{inmterchain}$ (d_3) in the real space are indicated.

side chains are of crystalline nature at room temperature. Morphology of thin polymer film of **2e** is viewed by means of the AFM image presented in Figure 7 as an example for the layered structures. In the figure, grains separated from each other by dark borders and without remarkable orientation correlation with the neighboring grains are seen. The clear stripes are attributed to the layers made of closely packed polymeric backbones **2e** separated by the side chains. Main chains are assumed to extend along the layer edges.

In Figure 8, distances corresponding to intramolecular correlations (when detected) as well as interlayer periods are plotted versus the molecular mass of the repeat unit (M^{ru}) along the backbone. This figure shows that correlations along polymeric backbones have nearly the same periodicity, but distances indicated by the equatorial reflections became larger by a factor nearly reflecting an increase of M^{ru}. Thus, polymeric backbones adopt a nearly regular extended conformation along the drawing direction, and lateral periodicity of the main chain related structure is controlled by the volume fraction of the aliphatic side segments.[24i] The location of the side chains along the RU does not influence the intramolecular correlations as well as layer spacing as proven by the nearly similar correlation distances obtained for **2c** and **2d**. The nearly linear increase of the layer spacings with M^{ru} (slope ≈ 1) indicates 1D dependence of the interlayer distances on side chain molecular mass fraction resulting from confinements of both the side chains and the main chains within the layered structure. The observed deviation may be rationalized by different packing modes of the side chains between backbone layers as well as deviation of the side chains from the all-trans conformation. Schematic illustration of the 3D molecular packing postulated for the bulk PPV/PPE in the oriented state as well as a schematic representation of the corresponding 2D fiber scattering pattern with contributions of effects related to the structure can be viewed in Figure 9. Some molecular parameters and structural dimensions of PPV/PPE are given in Supporting Information Table S1.

Because morphologies in bulk rely on the space filling conditions, interdigitation of side chains is presumed for the room-temperature structure of (PPV/PPE)s **2** leading to the translational correlation of the chains position along the filament axis. However, local organization of the side chains might be strongly dependent on their structural details, such as length, length distribution, and geometry of the grafted segments. For

example, from a comparison of experimental interlayer distances for **2e** and **2f** with simulated dimensions of fully extended dodecyloxy and octadecyloxy segments, interpenetrated packing of fully extended side chains oriented perpendicular to the chains axis is assumed.[30] However, the situation might differ slightly for (PPV/PPE)s **2a**−**d** having side chains of different lengths, for which limitation of side chain interpenetration may arise, for example, from the steric hindrance generated by the ethyl branching in the case of **2a**. The short spacing between two consecutive side chains extending from the same polymer chain of (PPV/PPE)s **1** is presumed to hinder interpenetration of side chains.[30c] If one takes into account these simple geometric considerations and the WAXS data obtained for **1b** regarded as the model compound for (PPV/PPE)s **1** owing to its equally long substituents, the end-to-end packing mode of the side chains tilted by about 65° with respect to the polymer backbone axis is considered.

All polymers have been subjected to thermal treatments in the oriented state and the structural changes have been examined. Here, we limit our discussion to the case of **2e** for which clear organizational variations have been detected with respect to its well-defined DSC traces (Figure 3). From a temperature of 453 K, three interrelated structural changes can be observed (Figure 6b): (1) The small-angle equatorial reflections are shifted toward smaller scattering vector positions, reflecting an increase of the layer spacing. Similar effects were also observed for other (PPV/PPE)s as indicated by the vertical arrows in Figure 8, the length of which scales with the observed displacement. (PPV/PPE)s **1** gave the shortest layer spacing increase, probably due to the presumed end-to-end packing mode as well as the less ordered nature of the side chains in the low-temperature phase in comparison to (PPV/PPE)s **2**. (2) A broad, diffuse halo appears at wide angles and represents a broad distribution of local interatomic distances between both confined side chain and main chain domains within the layered structure. (3) Meridional reflections lose their intensity. The last effect indicates that polymer chains become translationally uncorrelated within polymer backbone layers along the chain orientation direction because of the side chain disordering. These changes were perfectly reversible, and the X-ray intensity distributions recorded after cooling indicated 3D ordering with periods parallel and perpendicular to the chain axes.

Fluorescence Investigations on Extruded Filaments. Extruded filaments of polymers **1b** and **1d**, **2c** and **2d**, and **2e** and **2f** were purposely selected for fluorescence investigations with the aim of comparing their photoluminescent properties. All samples exhibited a very recordable fluorescence in the region between 500 and 750 nm. Excitation spectra were recorded in the wavelength region between 450 and 600 nm. Fluorescence and fluorescence excitation measurements were performed under a variation of excitation and emission wavelengths, respectively (Figure 10). For the purpose of comparison, normalized absorption and emission spectra for thin films spin-coated from chlorobenzene solutions are depicted in Figure 11.[23,24] As expected, a general red shift of the emission spectra going from the solutions over the thin films to the extruded fibers was observed (Table 2). This is attributed to enhanced planarization of the conjugated backbones and aggregate formation from the solutions

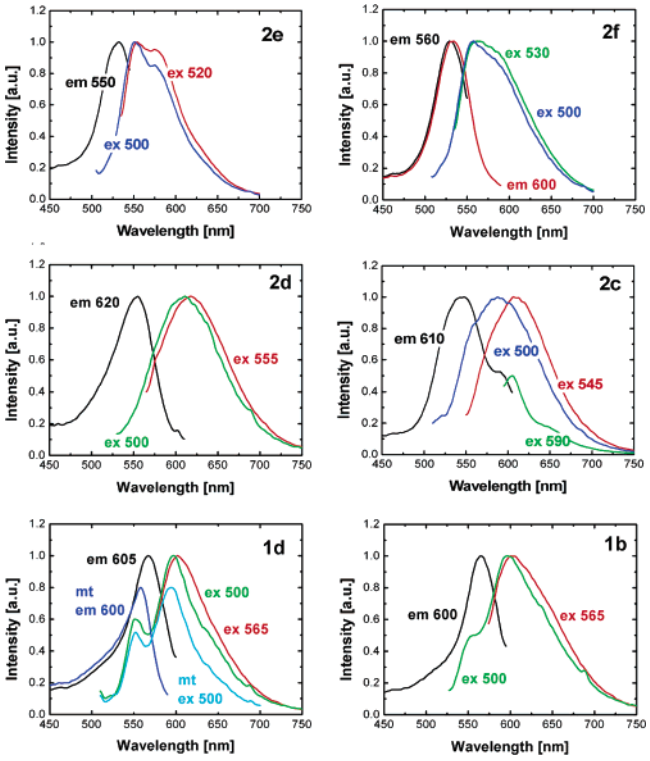

Figure 10. Normalized excitation and emission spectra of fibers of polymers **1b** and **1d**, **2c** and **2d**, and **2e** and **2f** obtained under frontal geometry experimental conditions.

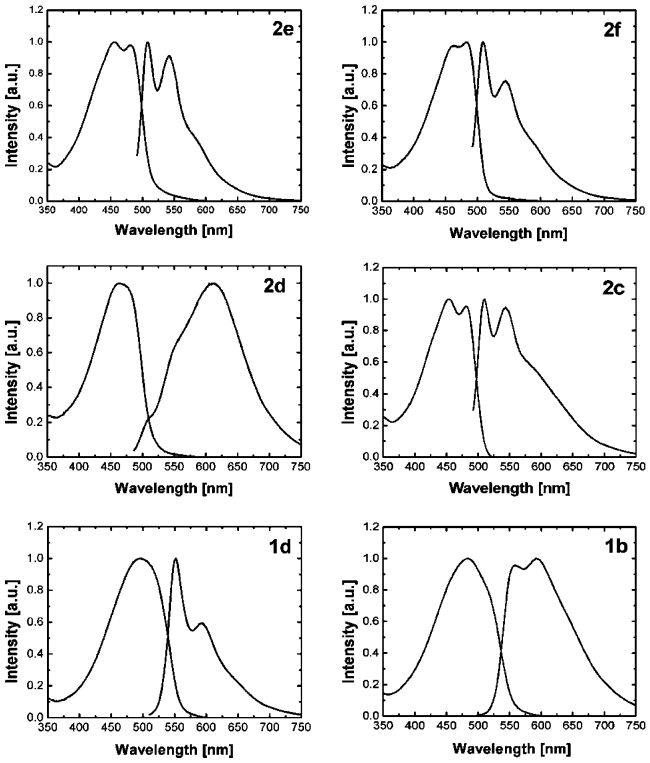

Figure 11. Normalized absorption and emission spectra of thin film of polymers **1b**, **1d**, **2c**, **2d**, **2e**, and **2f** casted from chlorobenzene solution.

to the compact bulk materials. Effect of side chain structural parameters as observed for the photoluminescent properties of polymer thin films[23] were reproduced for uniaxially oriented filaments, making it possible to gain insight into the structure−photophysi-

Table 2. Optical Data from Dilute Chloroform Solutions, Solid Films, and Fibers of Polymers 1b, 1d, 2c, 2d, 2e, and 2f

	$\lambda_{absorption}$ [nm]		$\lambda_{emission}$ [nm]		
polymer	solution	film	solution	film	fiber
1b	468	496	519	552, 592	601
1d	469	484	520	559, 593	602 (595) mt
2c	446	455, 483	489	510, 544	606
2d	446	465	490	610	618
2e	445	482	490	508, 542	553, 582
2f	447	486	490	509, 545	*562*, 590

cal property relationship of (PPV/PPE)s in the oriented state.

The fluorescence spectra of the first type of polymers, consisting of **2e** and **2f** bearing four equally long substituents, exhibit similar shapes with maxima around 550−560 nm and shoulders at 580−590 nm, which are approximately 40 nm red-shifted in comparison to thin film emission maxima. The maxima of the fluorescence excitation spectra were found between 510 and 530 nm. Fluorescence excitation and emission spectra of **2f** and **2e** exhibited only a minor dependence on the excitation and emission wavelengths chosen. Hence, the presence of essentially only one emitting species in the corresponding fibers is assumed. Polymer fibers extruded from the fourfold substituted compounds **2d** (R^2 = octadecyloxy, R^4 = octyloxy) and **2c** (R^2 = octyloxy, R^4 = octadecyloxy), having similar side chains but located at reversed positions along the chemical repeat units, showed broad, unstructured fluorescence spectra with maxima around 600 nm upon excitation at the maxima of the excitation spectra, which were found around 550 nm for both compounds. However, excitation at the long wavelength shoulder of **2c** yields a fluorescence spectrum (normalized to 0.5) with a maximum at 605 nm and a markedly smaller width. Excitation of both samples at a shorter wavelength (500 nm) resulted in essentially the same emission spectrum for **2d** but in a blue-shifted spectrum with a shoulder at 550 nm for **2c**. From these results, the existence of at least two emitting species within the fiber of **2c** is presumed. The shoulder emission around 550 nm can be ascribed to the isolated backbone fluorophore system, consistent with the peaks at 508 and 542 nm as obtained from the thin film emission. On the other hand, the main peak around 605 nm is presumed to reflect the excimer-like emission, resulting from enhanced planarization of the **2c** backbones and resulting from closer chain packing induced by the extrusion process. This assertion is supported by the change in color of the sample **2c** from yellow, as observed after polycondensation, to dark orange, as seen after extrusion (Figure 12). The variation in color was reversible, and **2c** recovered its original yellow color after being dissolved in chloroform solution. These macroscopic observations indicate that mechanical deformation induced only physical modifications within the polymer structure and does not affect the chemical structure of the polymer. In comparison to other polymers of type **2**, a near-overlap of the emission maxima is seen for the thin film and the extruded samples of **2d** (Figure 13). This might be interpreted in terms of strong self-assembly ability and concomitant planarization of the polymer backbone as suggested by the orange color of polymer **2d** obtained directly after the polycondensation reaction. Consequently, the extrusion process does not bring a significant change in the degree of backbone planarity. Thus, the specific positioning of

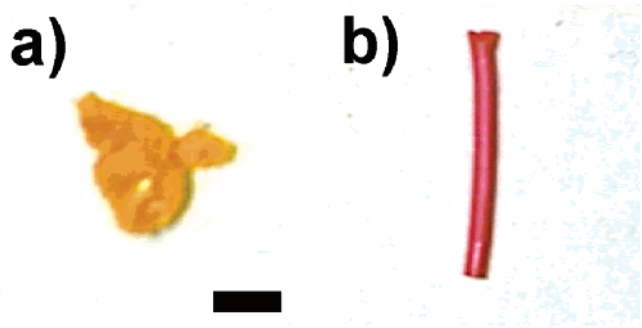

Figure 12. Micrographs of bulk samples of **2c** as obtained (a) after polymerization and (b) after extrusion. The black bar in the left figure represents size of 2 mm.

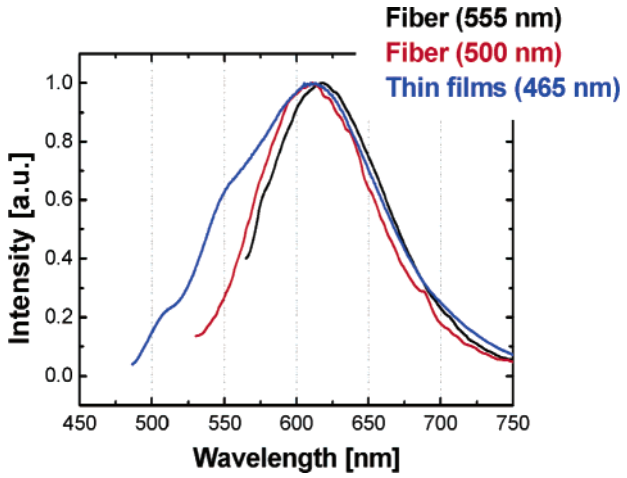

Figure 13. Superposition of thin film and fiber emission spectra of polymer **2d**. The excitation wavelength is indicated in the brackets.

octadecyloxy and octyloxy groups on the phenyl rings located between the ethynylene or vinylene units is a key parameter allowing the control of emission properties of (PPV/PPE)s π-conjugated backbones. Fluorescence and excitation data collected from the third group of polymer fibers, made of the eightfold alkoxy-substituted polymers **1d** and **1b**, exhibited a superposition of at least two distinguished emitting species with different intensities. Excitation at the maximum of the excitation spectra (∼565 nm) led to broad, unstructured fluorescence spectra with maxima detected at a wavelength value of about 600 nm. Lower-wavelength excitation (500 nm) resulted in a shoulder and a band at 550 nm for **1b** and **1d**, respectively.

As mentioned in the experimental part, measurements of emission and excitation spectra from microtome(mt)-sliced plane sections were also performed. Examples of such measurements can be viewed for **1d** (normalized to 0.8) in Figure 10 and Table 2. A very close similarity between these spectra and the ones recorded from the extruded sample indicates that the cylindrical shape of the filament does not significantly degrade the results obtained under our experimental conditions. Figure 14 presents a direct correlation between the photophysical and structural data collected for the extruded filaments. In this figure, the maximum wavelengths of the emission peaks are plotted versus the distances between the polymer chains within the layers. The nearly direct proportionality between these two bulk characteristics shows that packing of the main chains, which depends on the grafted side chains, controls the emission properties of (PPV/PPE)s **1** and **2**

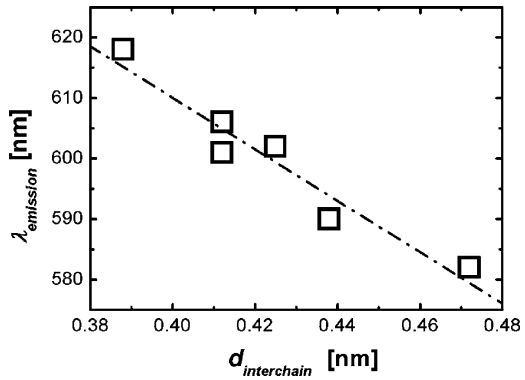

Figure 14. Dependence of the wavelengths of the emission maximum on the interchain distances within the layers for extruded filaments of **1b**, **1d**, **2c**, **2d**, **2e,** and **2f**.

in the oriented state. A close stacking of the main chains, as in the case of **2d**, may lead to a substantial bathochromic shift of the emission peak.

Conclusions

Some bulk properties of (PPV/PPE)s **1** and **2** differing in length, length distribution, location, density, and geometry of the grafted alkoxy side chains were examined in macroscopically isotropic and uniaxially oriented states. All the experimental results indicated a relatively strong dependence of their bulk characteristics on rather small variations of macromolecular architecture. Optically isotropic melts of eightfold substituted (PPV/PPE)s **1** crystallized through nucleation and growth leading to spherulitic morphologies, while fourfold substituted (PPV/PPE)s **2** underwent thermal degradation prior to isotropization. For all combinations of side chains, self-organization of hairy-rod macromolecules **1** and **2** within layered structures consisting of closely packed rigid main chain assemblies spatially confined by the flexible side chains controlling the space between backbone layers is proposed. The local arrangement of the side chains that depends mainly on the side chain density and temperature governs the type of ordering of the chains within the layers. Photoluminescence behavior of the extruded filaments was investigated, and a clear example is given for the control of optical properties of π-conjugated polymers by manipulating macromolecular order by means of mechanical deformation. Depending on the intrinsic self-assembly abilities of **1** and **2**, a bathochromic shift of the emission spectra was observed for the uniaxial orientation in comparison to thin films and solutions, due to enhanced planarization induced during the extrusion process. Side chain dependent correlation between the structure in the oriented state—interchain distances—and the photophysical parameters—wavelength of maximum emission—was finally established.

Acknowledgment. We thank R. Stimper and our students M. Metzner and M. Gericke for the preparation of the microtome sections. Moreover, we would like to dedicate this work to Prof. Dr. Tadeusz Pakula, who suddenly passed away while this manuscript was still under preparation, for his great contribution to the field of polymer physics. We shall all miss him.

Supporting Information Available: Table containing molecular parameters and structural dimensions of PPV/PPE. This material is available free of charge via the Internet at http://pubs.acs.org.

References and Notes

(1) (a) Blumstein, A.; Hsu, E. C. *Liquid Crystalline Order in Polymers*, Academic Press: New York, 1978. (b) Finkelmann, H.; Ringsdorf, H.; Wendorff, J. H. *Makromol. Chem*. **1978**, *179*, 273. (c) McArdle, C. B. *Side Chain Liquid Crystal Polymers*; Blackie and Son Ltd.: Glasgow, 1989.
(2) Roviello, A.; Sirigu, A. *J. Polym. Sci., Polym. Lett. Ed*. **1975**, *13*, 455.
(3) (a) Piao, X. L.; Sim, J.-S.; Yun, Y.-K.; Jin, J.-I. *Macromolecules* **1997**, *30*, 2294. (b) Ruan, J.; Ge, J. J.; Zhang, A.; Shi, J.; Wang, S.-Y.; Harris, F. W.; Cheng, S. Z. D. *Macromolecules* **2002**, *35*, 736.
(4) Platé, N. A.; Shibaev, V. P. *Comb-Shaped Polymers and Liquid Crystals*; Plenum Press: New York, 1987.
(5) Isayev, A. I.; Kyu, T.; Cheng, S. Z. D. *Liquid-Crystalline Polymer Systems. Technological advances*; ACS Symposium Series, American Chemical Society: Washington, DC, 1996.
(6) (a) Ballauf, M. *Makromol. Chem., Rapid Commun*. **1986**, *7*, 407. (b) Ballauf, M.; Schmidt, G. F. *Mol. Cryst. Liq. Cryst*. **1987**, *147*, 163. (c) Ballauf, M.; Schmidt, G. F. *Makromol. Chem., Rapid. Commun*. **1987**, *8*, 93.
(7) (a) Rodriguez-Parada, J. M.; Duran, R.; Wegner, G. *Macromolecules* **1989**, *22*, 2507. (b) Schrauwen, C.; Pakula, T.; Wegner, G. *Makromol. Chem*. **1992**, *193*, 11.
(8) (a) Watanabe, J.; Harkness, B. R.; Sone, M.; Ichimura, H. *Macromolecules* **1994**, *27*, 507. (b) Osada, K.; Niwano, H.; Tokita, M.; Kawauchi, S.; Watanabe, J. *Macromolecules* **2000**, *33*, 7420 (c) Fu, K.; Nematsu, T.; Sone, M.; Otoh, T.; Hayakawa, T.; Ueda, M.; Tokita, M.; Watanabe, J. *Macromolecules* **2000**, *33*, 8367.
(9) (a) Yamamoto, T.; Muramatsu, Y.; Lee, B.-L.; Kokubo, H.; Sasaki, S.; Hasegawa, M.; Yagi, T.; Kubota, K. *Chem. Mater*. **2003**, *15*, 4384. (b) Yamamoto, T.; Arai, M.; Kokubo, H.; Sasaki, S. *Macromolecules* **2003**, *36*, 7986.
(10) Neher, D. *Adv. Mater*. **1995**, *7*, 691.
(11) Hadziioannou, G., van Hutten, P. F., Eds. *Semiconducting Polymers: Chemistry, Physics and Engineering*, 1st ed.; Wiley-VCH: Weinheim, Germany, 2000.
(12) (a) Kraft, A.; Grimsdale, A. C.; Holmes, A. B. *Angew. Chem., Int. Ed*. **1998**, *37*, 402. (b) Friend, R. H.; Gymer, R. W.; Holmes, A. B.; Burroughes, J. H.; Marks, T. N.; Taliani, C.; Bradley, D. D. C.; Dos Santos, D. A.; Brédas, J. L.; Lögdlund, M.; Salaneck, W. R. *Nature (London)* **1999**, *397*, 121. (c) Schmitz, C.; Pösch, P.; Thelakkat, M.; Schmidt, H.-W.; Montali, A.; Feldman, K.; Smith, P.; Weder, C. *Adv. Funct. Mater*. **2001**, *11*, 41. (d) Pschirer, N. G.; Miteva, T.; Evans, U.; Roberts, R. S.; Marshall, A. R.; Neher, D.; Myrick, M. L.; Bunz, U. H. F. *Adv. Mater*. **2001**, *13*, 2691. (e) Sarker, A. M.; Gürel, E. E.; Ding, L.; Styche, E.; Lahti, P. M.; Karasz, F. E. *Synth. Met*. **2002**, *132* (3), 227.
(13) Pei, Q.; Yu, G.; Zhang, C.; Yang, Y.; Heeger, A. J. *Science* **1995**, *269*, 1086.
(14) Yang, Y.; Heeger, A. J. *Nature (London)* **1994**, *372*, 344.
(15) (a) Pauck, T.; Hernnig, R.; Perner, M.; Lemmer, U.; Siegner, U.; Mahrt, R. F.; Scherf, U.; Müllen, K.; Bässler, E. O.; Göbel, E. O. *Chem. Phys. Lett*. **1995**, *244*, 171. (b) Hide, F.; Diaz-Garcia, M. A.; Schwartz, B. J.; Andersson, M. R.; Pei, Q.; Heeger, A. J. *Science* **1996**, *273*, 1833.
(16) (a) Brabec, C. J.; Sariciftci, N. S.; Hummelen, J. C. *Adv. Funct. Mater*. **2001**, *11*, 15. (b) Piok, T.; Brands, C.; Neyman, P. J.; Erlacher, A.; Soman, C.; Murray, M. A.; Schroeder, R.; Graupner, W.; Heflin, J. R.; Drake, A.; Miller, M. B.; Wang, H.; Gibson, H.; Dorn, H. C.; Leising, G.; Guzy, M.; Davis, R. M. *Synth. Met*. **2001**, *116*, 343.
(17) (a) Burroughes, J. H.; Bradley, D. D. C.; Brown, A. R.; Marks, R. N.; MacKays, K.; Friend, R. H.; Burn, P. L.; Holmes, A. B. *Nature (London)* **1990**, *347*, 539. (b) Greenham, N. C.; Moratti, S. C.; Bradley, D. D. C.; Friend, R. H.; Holmes, A. B. *Nature (London)* **1993**, *365*, 628. (c) Moratti, S. C.; Cervini, R.; Holmes, A. B.; Baigent, D. R.; Friend, R. H.; Greenham, N. C.; Grüner, J.; Hamer, P. J. *Synth. Met.* **1995**, *71*, 2117. (d) Lux, A.; Holmes, A. B.; Cervini, R.; Davies, J. E.; Moratti, S. C.; Grüner, J.; Cacialli, F.; Friend, R. H. *Synth. Met*. **1997**, *84*, 293.
(18) (a) Gurge, R. M.; Sarker, A.; Lahti, P. M.; Hu, B.; Karasz, F. E. *Macromolecules* **1996**, *29*, 4287. (b) Pinto, M. R.; Hu, B.; Karasz, F. E.; Akcelrud, L. *Polymer* **2000**, *41*, 2603.
(19) Hörhold, H.-H.; Helbig, M. *Makromol. Chem., Makromol. Symp*. **1987**, *12*, 229.
(20) (a) Bunz, U. H. F. *Chem. Rev*. **2000**, *100*, 1605. (b) Brizius, G.; Pschirer, G. N.; Steffen, W.; Stitzer, K.; zur Loye, H.-C.; Bunz, U. H. F. *J. Am. Chem. Soc.* **2000**, *122*, 12435. (c)

Wilson, J. N.; Windscheif, P. M.; Evans, U.; Myrick, M. L.; Bunz, U. H. F. *Macromolecules* **2002**, *35*, 8681.
(21) Ramos, A. M.; Rispens, M. T.; van Duren, J. K. J.; Hummelen, J. C.; Janssen, R. A. J. *J. Am. Chem. Soc.* **2001**, *123*, 6714.
(22) (d) Schenning, A. P. H.; Tsipis, A. C.; Meskers, S. C. J.; Beljonne, D.; Meijer, E. W.; Brédas, J. L. *Chem. Mater.* **2002**, *14*, 1362.
(23) (a) Egbe, D. A. M.; Tillmann, H.; Birckner, E.; Klemm, E. *Macromol. Chem. Phys.* **2001**, *202*, 2712. (b) Egbe, D. A. M.; Roll, C. P.; Klemm, E. *Des. Monomers Polym.* **2002**, *5*, 245. (c) Egbe, D. A. M.; Roll, C. P.; Birckner, E.; Grummt, U.-W.; Stockmann, R.; Klemm, E. *Macromolecules* **2002**, *35*, 3825. (d) Egbe, D. A. M.; Birckner, E.; Klemm, E. *J. Polym. Sci., Part A: Polym. Chem.* **2002**, *40*, 2670.
(24) (a) Egbe, D. A. M.; Cornelia, B.; Nowotny, J.; Günther, W.; Klemm, E. *Macromolecules* **2003**, *36*, 5459. (b) Ding, L.; Egbe, D. A. M.; Karasz, F. E. *Macromolecules* **2004**, *37*, 6124. (c) Egbe, D. A. M.; Stockmann, R.; Hotzel, M. *J. Opt. A: Pure Appl. Opt.* **2004**, *6*, 791. (d) Egbe, D. A. M.; Carbonnier, B.; Ding, L.; Mühlbacher, D.; Birckner, E.; Pakula, T.; Karasz, F. E.; Grummt, U.-W. *Macromolecules* **2004**, *37*, 7451. (e) Hoppe, H.; Egbe, D. A. M.; Mühlbacher, D.; Sariciftci, N. S. *J. Mater. Chem.* **2004**, *14*, 3462. (f) Egbe, D. A. M.; Kietzke, T.; Carbonnier, B.; Mühlbacher, D.; Hörhold, H.-H.; Neher, D.; Pakula, T. *Macromolecules* **2004**, *37*, 8863. (g) Al-Ibrahim, M.; Konkin, A.; Roth, H.-K.; Egbe, D. A. M.; Klemm, E.; Zhokhavets, U.; Gobsch, G.; Sensfuss, S. *Thin Solid Films* **2005**, *474*, 201. (h) Konkin, A. L.; Sensfuss, S.; Roth, H.-K.; Nazmutdinova, G.; Schroedner, M.; Al-Ibrahim, M.; Egbe, D. A. M. *Synth. Met.* **2005**, *148*, 199. (i) Carbonnier, B.; Pakula, T.; Egbe, D. A. M. *J. Mater. Chem.* **2005**, *15*, 880.
(25) (a) Wadsworth, W. S. *Org. React.* **1977**, *25*, 73. (b) Maryanoff, B. E.; Reitz, A. B. *Chem. Rev.* **1989**, *89*, 863. (c) Hörhold, H.-H.; Opfermann, J. *Makromol. Chem.* **1970**, *131*, 105.
(26) Guinier, A. *X-ray Diffraction in Crystals, Imperfect Crystals and Amorphous Bodies*; W. H. Freeman and Co.: San Francisco, 1963.
(27) Stein, R. S.; Rhodes, M. B. *J. Appl. Phys.* **1960**, *31*, 1873.
(28) Kakudo, M.; Kasai, N. *X-ray Diffraction by Polymers*; Kodansha: Tokyo, 1972.
(29) Carbonnier, B.; Andreopoulou, A. K.; Pakula, T.; Kallitsis, J. K. *Macromol. Chem. Phys*. **2005**, *206*, 66. Andreopoulou, A. K.; Carbonnier, B.; Kallitsis, J. K.; Pakula, T. *Macromolecules* **2004**, *37*, 3576.
(30) (a) Swan, P. R. *J. Polym. Sci*. **1962**, *56*, 403. (b) Jordan, E. F.; Feideisen, D. W.; Wrigley, A. N. *J. Polym. Sci., Part A-1* **1971**, *9*, 1835. (c) Hsieh, H. W.; Post, B.; Morawetz, H. *J. Polym. Sci., Polym. Phys. Ed*. **1976**, *14*, 1241.

MA0513160